

STUDY OF THE TOW BUCKLING DEFECT DURING THE COMPLEX SHAPE FORMING OF SYNTHETIC AND VEGETAL FIBRE REINFORCED STRUCTURAL COMPOSITES

M.M. Salem, E. De Luycker, M. Fazzini and P. Ouagne

Laboratoire Génie de Production (LGP), INP-ENIT, Univ. de Toulouse, Tarbes, France

Abstract: Fibrous reinforcements for structural composites manufacturing need to undergo in certain cases a complex shape forming process during which multiple defects could appear. These defects, such as tow buckling and tow sliding may reduce the integrity of the final part. The onset of these defects depends on the initial loading conditions, the shape of the preform and the characteristics of the textile material. While mechanisms behind the formation and development of both defects are yet to be fully understood. We focused, in this work, on investigating the buckling defect. In order to do so, we used optical field measurement techniques to monitor the kinematics of the defect appearance and predict it via an adapted analytical model of the defect appearance.

Key words: Composite manufacturing, preforming defects, textile reinforcement, tow buckling, full field strain measurement.

1 INTRODUCTION

Fibre reinforced composites receive an ever growing interest, because of their interesting mechanical properties, low cost and progressively mastered manufacturing techniques [1]. The complex shape forming of fibre reinforced composites might be done using techniques such as Resin Transfer Molding or Thermoplastic-Matrix Composites Stamping to produce seamless materials [2] but it can be less productive than regular laminates and susceptible to produce defects that alter the mechanical properties of the composite [3].

Thus, it is essential to fully understand and anticipate the appearance of defects such as the tow buckling which will be the focus of this paper. In the literature, the buckling defect appears on woven reinforcements and seems to be the result of the in-plane bending of the tows coupled with initial loads and reinforcement properties. Thus a buckling device, presented in Figure 1, was designed and manufactured to reproduce those conditions in a controlled environment [4].

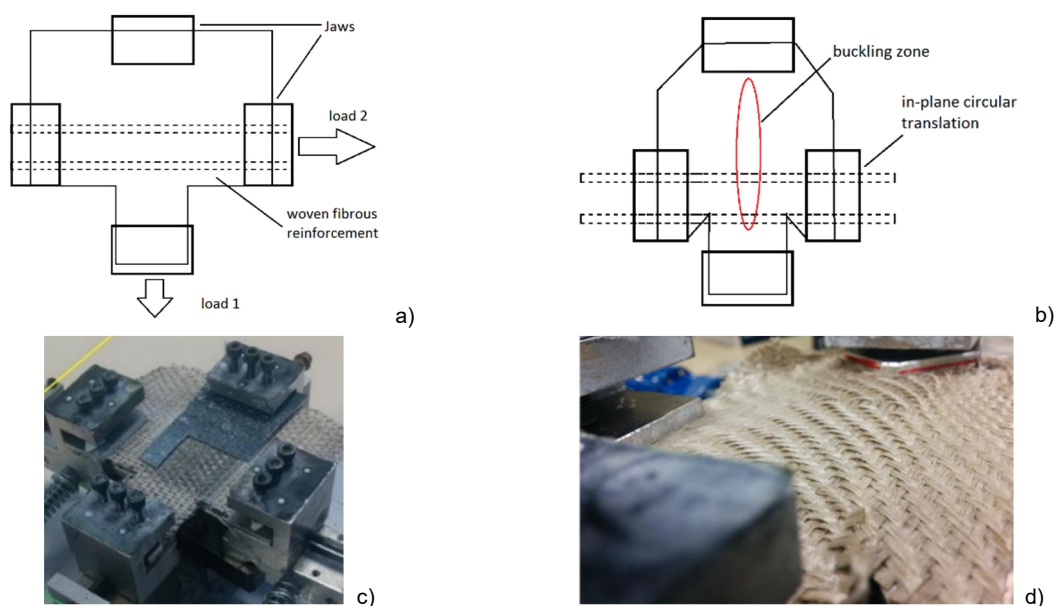


Figure 1 Buckling device principle a), b); Appearance of the buckles on the bent reinforcement surface c), d)

2 EXPERIMENTAL STUDY

2.1 Description of the buckling device

The buckling device is instrumented with two load cells, one in each direction of the weave in order to monitor the applied load. The buckling device was also equipped with a digital image correlation camera in order to record the bending angle between the tow's initial position and the bent state at any given moment. T shape samples were loaded in the device. This allowed the in-plane bending of one network (the transverse one) up to a 40° bending angle from the initial tow position (Figure 1b).

Furthermore, three full field optical systems: Various-focus microscopy (Figure 2a), Fringe projection (Figure 2b) and Stereo-Digital Image Correlation (Figure 2c), were considered and tested to assess the formation of the buckle. Three tests were performed in similar conditions as it is impossible to combine the optical systems equipments. The reconstructed surfaces of the tows from each technique are presented in Figure 2.

The profiles of the tow buckle (red lines in Figure 2) at the initial state 0° and after an in-plane bending

angle of 25° are given in Figure 3 for the three reinforcements tested with the three full field optical systems. One can globally see that the three techniques indicate relatively similar profiles and thus results from each technique can be considered valid. The S-DIC was finally chosen as it allows both fast and accurate enough results plus native displacement data.

2.2 Buckling tests

Three different reinforcements, listed in Table 1, were tested. Some of their geometrical characteristics are also given in Table 1. The influence of multiple parameters, such as initial loading in both weave directions as well as the reinforcement mechanical and geometrical properties, is considered. In the following, the bending rigidity and tow's geometries were investigated. The reinforcements were subjected to a 300 N load in the fixed tows network and 20 N in the bending tows network and bent up to 40° angle. Figure 4 shows the evolution of the maximum tow elevation as a function of the in-plane bending angle.

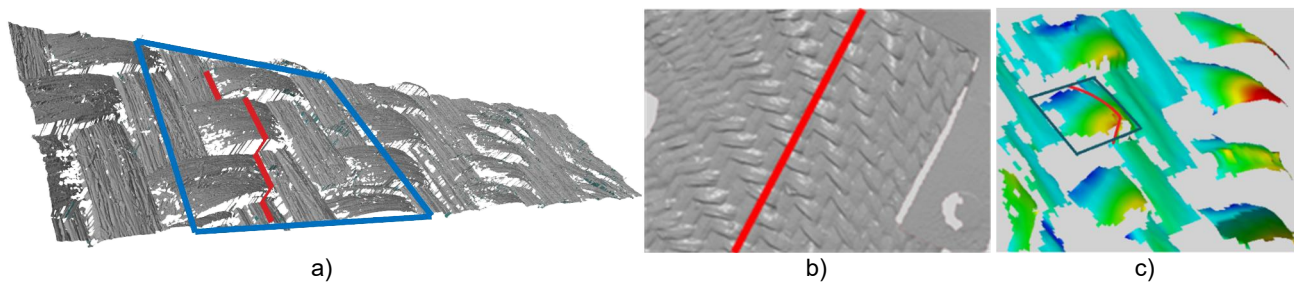


Figure 2 Reconstructed surface and profile of the tows (red line) obtained by focus-variation microscopy (a), fringe projection (b) and Stereo-digital image correlation (S-DIC) (c)

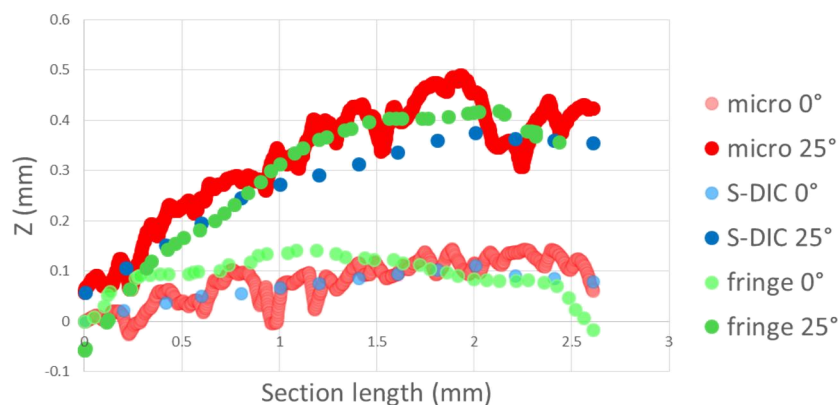


Figure 3 Buckles profiles comparison using stereo-DIC, Fringe projection and Various-focus microscopy at tow bending angles of 0° and 25°

Table 1 Characteristics of reinforcement used for tow buckling

Weave	Material	Area density [g/m ²]	Warp density [m ⁻¹]	Weft density [m ⁻¹]	Unsupported length [mm]	Unsupported width [mm]	Tow bending rigidity [N.mm]
Twill 2x2	Sized up linen	476	380	385	6.1	2.5	1.18
Twill 2x2	De-sized up linen	465	380	430	5.7	2.4	0.72
Twill 2x2	Carbon fiber	600	380	380	6.4	2.3	7.55

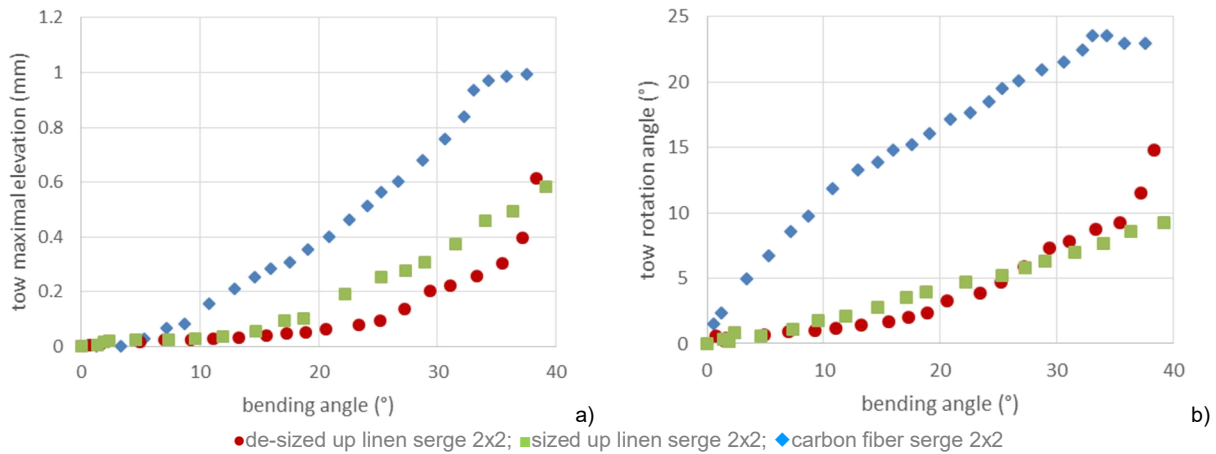


Figure 4 Maximum elevation (a) and rotation angle of the tow (b) as a function of the bending angle

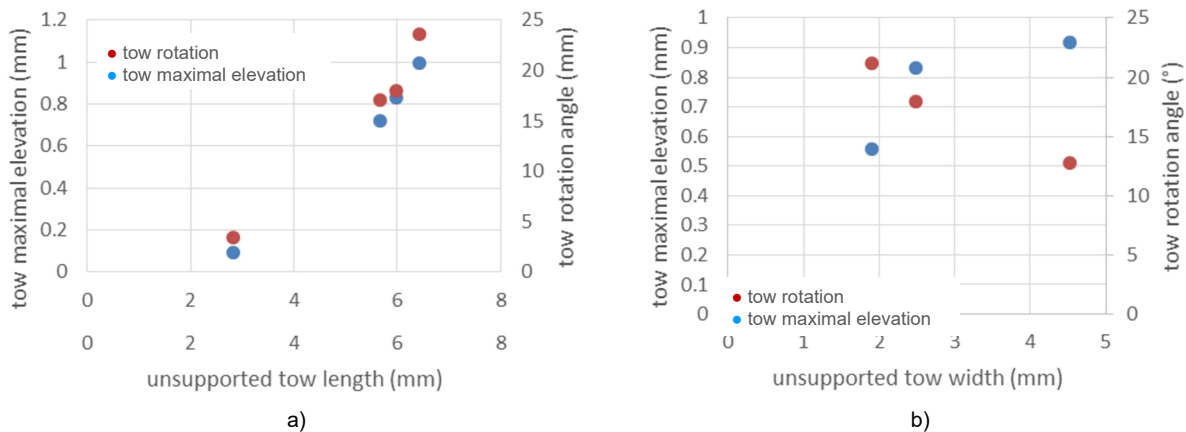


Figure 5 Maximum elevation and rotation angle of the tow as a function of the unsupported tow length (a) and as a function of the unsupported tow width (b)

One can observe in Figure 4 that the buckles appear for lower in-plane bending angles for the carbon twill weave. For the carbon reinforcement we notice the onset of the buckle at a bending angle of 5°, followed by the sized-up linen reinforcement at an angle of 10° and finally by the desized-up linen reinforcement at an angle of 13°. As the bending rigidity (measured independently on an adapted system) decreases the onset of the buckle is much more delayed and the size of the final buckle is smaller. Since the tows are under displacements constraints, the load repartition for the same bending angle is different depending on the material. More rigid tows achieve a critical buckling load for lower

values of bending angles which explains the earlier buckling. Consequently, the bending rigidity of the tow for relatively similar contexts and tow geometries is therefore a key parameter that controls the appearance and the evolution of the tow buckling defect.

As for the effect of tows geometry, taking into account the variation of the unsupported length and width of the tows and using the same experimental conditions as before, we compared for a de-sized up linen based reinforcements the impact of the unsupported tow length (the length for a given architecture between two weft perpendicular tows) and the unsupported tow width (the width of the tow

showing the in-plane bending (the warp tow) in Figure 5. As the unsupported length grows in Figure 5a, so does the tow deflection and rotation. This is explained by the added freedom for the buckle to rise and develop. But as the unsupported width grows in Figure 5b, the deflection grows while the rotation diminishes. This could be explained by smaller size buckles compared to the tow width, which means even if they deflect higher, the deflection compared to the tow width seems to be declining.

3 ANALYTICAL MODEL

An analytical framework based on the buckling of orthotropic homogenous plate is proposed to predict the buckling of tows inspired from a work made for tape on an elastic foundation for the buckling of steered tows in automated dry fibre placement [5]. Considering the tow as an orthotropic thin plate [6], the differential equation for plate bending, was solved by using the Rayleigh-Ritz approach. This approach allows us to determine the critical buckling load P_{cr} , for which the tow starts to deflect:

$$P_{cr} = \frac{\frac{24D_{11}m^2\pi^2}{L^2} + \frac{90D_{22}L^2}{b^4m^2\pi^2} + \frac{160D_{66}}{b^2} - \frac{40D_{12}}{b^2}}{6 - \alpha} \quad (1)$$

where D_{11} is the bending stiffness in the longitudinal direction, D_{22} is the bending stiffness in the transversal direction, D_{12} is the Poisson-action bending stiffness, D_{66} is the torsional stiffness, L is the tow length, b is the tow width, m is the buckling mode and α is the non-uniformity load coefficient which characterize the bending - tension combination (2 for pure bending and 0 for pure compression) as illustrated in Figure 6.

By equating P_{cr} to the minimal buckling load on the inner edge of the tow, P_0 defined geometrically in equation 2, the critical curvature radius for buckling, R_{cr} , was identified in equation 3.

$$P_0 = \frac{E1 h b}{\alpha R} \quad (2)$$

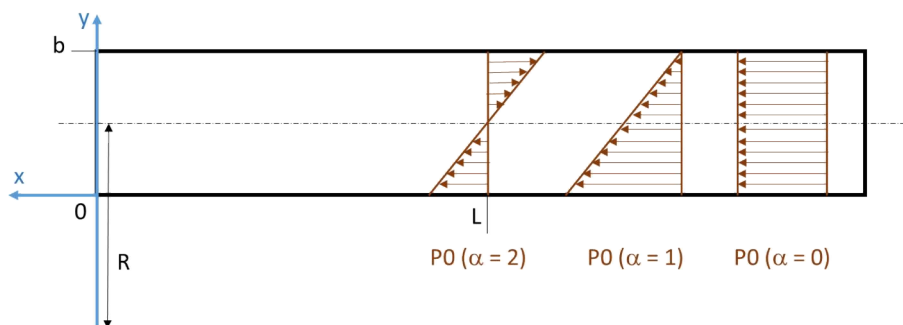


Figure 6 Tow representation from above as an orthotropic plate with compressive load P_0 ; representation for different values of the non-uniformity coefficient α

$$R_{cr} = \frac{E1(6 - \alpha)bh}{\alpha \left(\frac{24D_{11}m^2\pi^2}{L^2} + \frac{90D_{22}L^2}{b^4m^2\pi^2} + \frac{160D_{66}}{b^2} - \frac{40D_{12}}{b^2} \right)} \quad (3)$$

where $E1$ is the longitudinal tensile modulus and h is the thickness of the tow.

As stipulated in [5], D_{12} and D_{22} are orders of magnitude lower than D_{11} and D_{22} and thus can be neglected with close to no impact on the critical radius, thus, the expression of R_{cr} becomes:

$$R_{cr} = \frac{E1(6 - \alpha)b^3hL^2}{\alpha(160 D_{66} L^2 + 24 D_{11} \pi^2 b^2 m^2)} \quad (4)$$

The bending stiffness D_{11} was then evaluated using a Peirce cantilever test and the torsional stiffness was evaluated using a torsion test. α was also estimated using digital image correlation. This finally allowed us to calculate the critical buckling radius and compare it to the experimental buckling radius that was measured experimentally using ImageJ® on the previously mentioned digital image correlation pictures. $E1$ was retrieved from the literature as the used tows resemble those used by Bassoumi [7] in her work. All the results are compiled in Table 2.

Table 2 Parametric results, analytical and experimental critical radii

Reinforcement	Serge 2x2 sized up	Serge 2x2 de-sized up
E1 [N/mm²]	19800	7800
L [mm]	6.1	5.7
b [mm]	2.5	2.4
h [mm]	0.4	0.4
α	2	2
m	1	1
D11 [N.mm]	1.18	0.72
D66 [N.mm]	0.44	0.17
Rcr [mm]	2082.9	1482.2
Rcr(exp) [mm]	2255	1627
Δ [%]	7.63	8.90

The analytical and experimental results seem to be in agreement with only 8.2% difference so we can assume that the model can safely predict the critical buckling radius. Yet, more reinforcement needs to be studied in order to confirm the results.

4 CONCLUSION

The tow buckling defect was investigated using a specifically made device and some parameters were studied. The effect of tows dimensions and tow rigidities was experimentally studied and related to the buckling. An analytical framework was adapted from the literature and was found to be able to predict the critical buckling radius so far with a need for further tests on different reinforcements to fully validate it.

5 REFERENCES

1. Pickering K.L., Aruan Efendy M.G., Le T.M.: A review of recent developments in natural fibre composites and their mechanical performance, *Composites Part A: Applied Science and Manufacturing* 83, 2016, pp. 98-112, <https://doi.org/10.1016/j.compositesa.2015.08.038>
2. Boisse P.: Mise en forme des renforts fibreux de composites, *Techniques de l'ingénieur*, Réf: AM3734 v1, 2004, pp. 1-10, <https://www.techniques-ingenieur.fr/base-documentaire/materiaux-th11/plasturgie-procedes-specifiques-aux-composites-42474210/mise-en-forme-des-renforts-fibreux-de-composites-am3734/>
3. Potter K., Khan B., Wisnom M., Bell T., Stevens J.: Variability, fibre waviness and misalignment in the determination of the properties of composite materials and structures, *Compos. Part A: Applied Science and Manufacturing* 39(9), 2008, pp. 1343-1354, <https://doi.org/10.1016/j.compositesa.2008.04.016>
4. Tephany C.: Analyse de la formabilité de renforts composites à base de fibres naturelles, PhD thesis, Université d'Orléans, 2014
5. Matveev M.Y., Schubel P.J., Long A.C., Jones I.A.: Understanding the buckling behaviour of steered tows in Automated Dry Fibre Placement (ADFP), *Composites Part A: Applied Science and Manufacturing* 90, 2016, pp.451-456, <https://doi.org/10.1016/j.compositesa.2016.08.014>
6. Florimond C.: Contributions à la modélisation mécanique du comportement de mèches de renforts tissés à l'aide d'un schéma éléments finis implicite, INSA-Lyon, 2013
7. Bassoumi A.: Analyse et modélisation du choix des renforts pour optimiser la mise en forme de matériaux composites à base de fibres végétales, PhD thesis Université d'Orléans, 2016